

Christian Cornelius

Siemens AG,
Energy Sector,
Fossil Power Generation Division,
Mellinghofer Str. 55,
Mülheim an der Ruhr 45473, Germany

Thomas Biesinger

Siemens AG,
Energy Sector,
Fossil Power Generation Division,
Mellinghofer Str. 55,
Mülheim an der Ruhr 45473, Germany

Paul Galpin

ANSYS Canada Ltd.,
283 Northfield Drive E, Unit 21,
Waterloo, ON N2J 4G8, Canada

André Braune

ANSYS Germany GmbH,
Staudenfeldweg 12,
Otterfing 83624, Germany

Experimental and Computational Analysis of a Multistage Axial Compressor Including Stall Prediction by Steady and Transient CFD Methods

Siemens Energy has commissioned an extensive multiyear experimental and numerical (computational fluid dynamics (CFD)) project to improve its ability to design for and predict compressor stall. The experimental test rig is a half scale six stage axial compressor. The goal of this work is to provide insight into how best to predict the compressor performance map and in particular the stall point by applying state-of-the-art multiple blade row CFD simulation tools. A preliminary CFD analysis quantified numerical, model, and systematic error on the first stage of the compressor. Subsequent steady (mixing plane) and transient (time transformation) CFD simulations of the entire six stage compressor are compared to each other and to experimental data. Both the steady and transient simulations are shown to be computationally efficient and in very good agreement with the experimental data across the full performance map, up to stall inception on multiple speedlines. Physical explanations of the key flow features observed in the experiment, as well as of the differences between the predictions and experimental data, are given.

[DOI: 10.1115/1.4025583]

Introduction

The demand for improved compressor efficiency and increased blade loading requires advanced CFD simulations that can reliably predict the impact of design modifications on the efficiency and also the aerodynamic stability at critical operating points. CFD methods are well established for predicting multistage compressor performance near the design point (e.g., Belamri et al. [1], Ikeguchi [2]) but less so toward stall and the aerodynamic stability limit. Compressor stall and surge is highly complex and unstable and occurs in different forms, including modal or rotating stall (Mailach and Vogeler [3]) and spike stall (Camp [4], Courtiade and Ottavy [5]). While it is important to understand the flow physics as a compressor stalls and surges, in practice the designer needs only to predict the point of numerical peak pressure ratio, with no real need to resolve the flow details during the actual breakdown process of surge.

To be of practical use, a computationally robust and efficient CFD stall prediction methodology is needed. As compressor stall is a system effect determined by the specific characteristics of all stages and their interaction rather than a local effect, it requires multistage analysis. Examining the stall behavior of isolated rotors is useful but does not necessarily indicate the stall point for the compressor. In general multirow turbomachinery flow is unsteady, but the onset of stall is fundamentally a transient phenomenon. It involves both self-excitation at blade passing frequencies and their interactions, often even without single passage periodicity. All of these factors limit the ability of steady methods (e.g., mixing plane) to predict stall, and prompt the consideration of transient CFD methods, and their associated increase in computational effort.

Use of transient CFD analysis for stall and stability prediction raises many additional questions, such as when are steady methods no longer appropriate and what level of detail must be resolved in a transient simulation to accurately predict the onset of stall? Two new critical modeling issues arise: How does one efficiently deal with the pitch change (what extent of the 360 deg of the machine is solved) and how is turbulence modeled given the transient flow conditions (e.g., with time-diffusive unsteady Reynolds-averaged Navier-Stokes (URANS) or with expensive scale resolving methods such as large eddy simulation (LES))? While it is theoretically possible to resolve all blade passages in 360 deg this is impractical for industrial compressors consisting of perhaps 15 or more compressor stages with more than 100 blades per row in the rear stages. Methods that limit the modeled blade count to one or a few passages per row are mandatory, but these methods must still assume the flow repeats each blade passage (e.g., rotating instabilities are precluded). The current work makes no attempt to resolve any large scale flow asymmetry such as rotating stall due to the assumption of repeating flow pattern per passage inherent in the single blade pitch change methods employed. It is the subject of future work to predict rotating stall and, hence, be able to assess its impact on the stability prediction.

To be computationally efficient yet accurate is a major challenge for stability predictions. Ideally a modest spatial (mesh) and temporal (time step) step is desired for computational speed, at odds with the flow complexity near stall. Due to the unstable nature of the flow at stall conditions small details of the model, e.g., tip clearances, fillets, exit, bleed, and leakage modeling can have a significant impact on the prediction.

The objective of this paper is to make progress toward answering some of the above questions, keeping in mind that a designer requires timely stall predictions from the analysis. The case used is a Siemens six stage axial compressor, but it is likely that the observations and methods developed are applicable to other compressor designs. Sensitivity of predictions to numerical, model and systematic error are explored on the first stage of the

Contributed by the International Gas Turbine Institute (IGTI) of ASME for publication in the JOURNAL OF TURBOMACHINERY. Manuscript received July 4, 2013; final manuscript received July 18, 2013; published online November 28, 2013. Editor: Ronald Bunker.

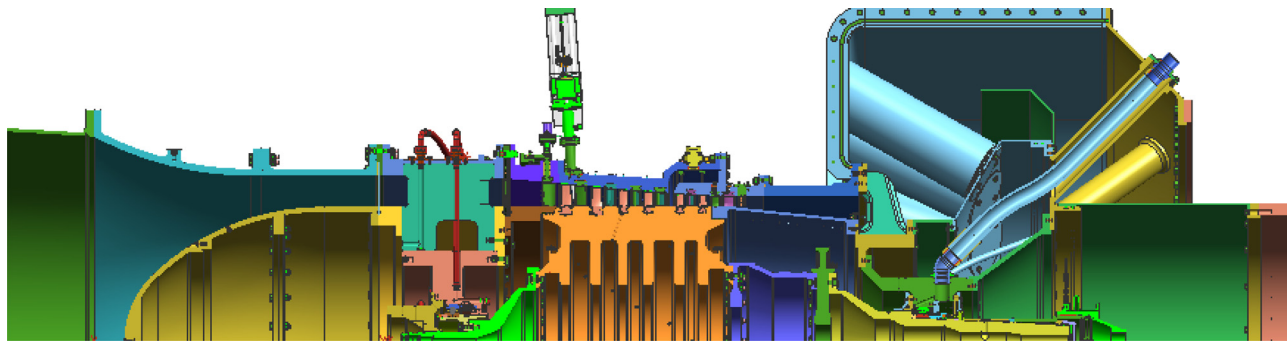


Fig. 1 Meridional view of the Siemens PCO rig (1/2) scale six stage axial compressor

compressor. Based on knowledge gained from the preliminary study, the full six stage compressor is then modeled using steady and time accurate transient methods. Predictions are obtained on three speedlines (85%, 100%, 120%), and comparison is made between the methods and experimental data.

Experimental Rig. Siemens has commissioned an extensive multiyear experimental and numerical (CFD) project to improve their ability to predict compressor aerodynamic stability. The six stage half scale compressor test rig (“PCO Rig”) comprises the last five stages of the Siemens platform compressor (PCO) and is equipped with a variable inlet guide vane to adjust the operating characters of the first stage, as shown in Fig. 1. The initial build I features blading with high performance airfoils (HPA airfoils), a Siemens-proprietary family of compressor airfoils optimized for the conditions in the rear stages of large heavy duty gas turbine compressors [6,7]. The overall pressure ratio exceeds 2.5. The stator blades are cantilevered. Build I tip gaps are by design relatively small, being about 1% of the blade height.

The purpose of the rig is to generate experimental data for determining the aerodynamic performance including surge margin of the compressor, as well as to investigate the effects of various design factors (e.g. effect of tip clearance variation, and so forth). The rig consists of an inlet guide vane (IGV), followed by 6 stages, an outlet guide vane, and an outlet diffuser section including a simplified combustion system, shown in Fig. 1. Blade counts range from approximately 70 to 120 blades per rotor. There is an outer bleed downstream of Stator 4 and two hub leakages at the first and last disk of the rotor. Experimental data is available for the overall compressor characteristics (mass flow, pressure ratio, efficiency) as well as local flow measurements (Pttotal and Ttotal rakes at inlet and exit and at the leading edge of all vanes). In addition, fast (Kulite) pressure measurements were taken over blade tips to identify stall inception. Experiments were performed for several maps with different bleeds, inlet pressures and turbulence screens, for speedlines ranging from 85% to 125%. Data was collected along each speedline at 10–15 operating points up to the experimentally determined surge. Surge points shown in this paper are based on time averaged data for the last stable operating point of the compressor. Unsteady measured surge points based on fast sensors are usually within a 1% range. The uncertainty of the measured mass flow is lower than 1%.

Computational Method

CFD Solver. All CFD simulations are performed with ANSYS CFX version 14.5 [8]. The CFX flow solver is an unstructured multiple element (hex, tet, wedge, pyramid) finite volume method. Primitive variables for velocity, pressure, enthalpy, etc are defined at nodes at the corners of each element. Conservation equations are obtained by integration over the element mesh-dual. Second order accurate discretizations are used. A fully implicit solution strategy is employed. Multigrid acceleration is applied to the

coupled solution of the governing equations (Raw [9]). A domain decomposition method is employed to permit parallel processing.

Rotor Stator Modeling. Compressor simulations involve rotating and stationary blading components within a single simulation. Rotors are solved in the rotating frame of reference while all other components (stators, guide vanes, bleeds, etc.) are in a stationary frame of reference. Interfaces connect the two frames of reference. The type of interface used defines the type of rotor-stator simulation. A steady rotor-stator CFD simulation is obtained when mixing planes (MP) are defined between each rotor/stator pair. In this approach all transported quantities (mass, momentum, energy, turbulence, etc.) are conserved but mixed-out while crossing the interface, to support steady flow in each frame of reference. The circumferential averaging procedure is implemented in an implicit fashion for robust convergence. Instantaneous periodicity and pitch change are naturally supported by the Mixing Plane interface. The procedure has been validated and applied to a wide range of turbomachinery [8].

A transient rotor-stator simulation involves a time accurate interface between rotor and stator that is updated each time step as the relative position of the two blades change. Transient rotor-stator (TRS) interface methods differ in how pitch change is handled between adjacent blade rows. A pitch change resulting from different blade row numbers requires a method to achieve periodicity for a single passage. In this investigation two different TRS methods within a family of “transformation methods” are used, namely profile transformation (PT), Galpin et al. [10], and time transformation (TT, Giles [11] and Connell et al. [12]). These methods have recently been validated for a range of flow conditions and pitch change (Biesinger et al. [13]). They have been shown to accurately and efficiently reproduce full wheel transient simulations solving just one passage per blade row.

The PT method involves an interface flux scaling procedure. Flow profiles are circumferentially stretched or compressed across the rotor-stator interface, maintaining conservation and consistency with the imposed instantaneous periodicity for each blade. In the case of equal pitch the PT method becomes exact. The PT model error increases with pitch ratio but is managed by solving two or more blade passages per component to bring the ensemble pitch ratio closer to unity. The PT method is fully implicit, robust, and applicable to multistage. The main modeling error with the PT method is a distortion in frequency of temporal disturbances crossing the rotor-stator interface.

The TT method builds on the PT method (instantaneous periodicity, circumferential profile scaling at the interface) but with a key difference. Physical time varies linearly in the pitchwise direction in proportion to the pitch ratio as originally conceived of by Giles [11], such that instantaneous periodicity and profile scaling within the computational time plane becomes exact even for pitch change. The TT implementation retains the advantages of the PT method (implicit, conservative) but without frequency distortion at the interface (temporal disturbances are accurately

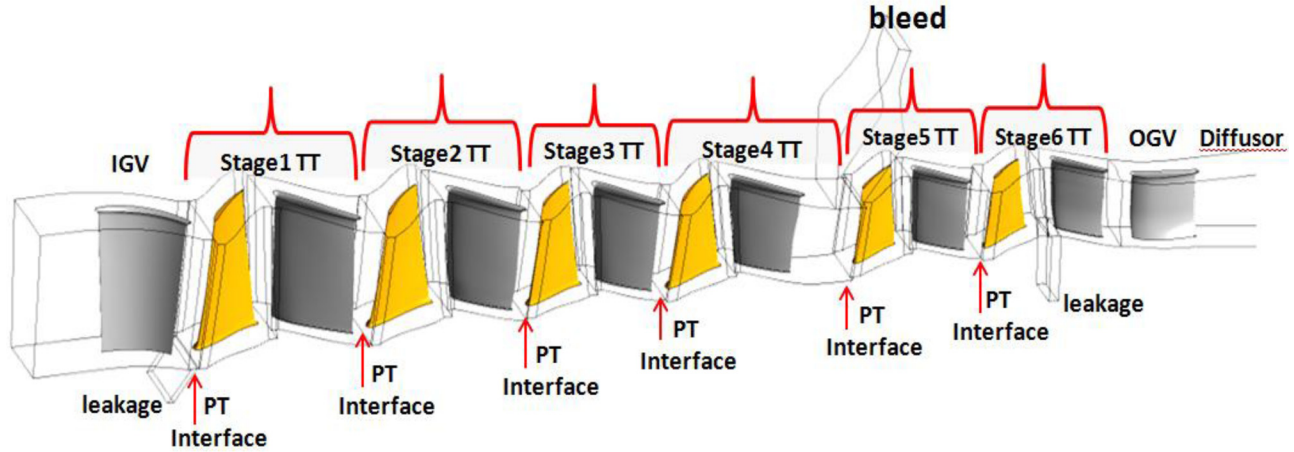


Fig. 2 Multistage transient model using time transformation for each stage, connected with profile transformation interfaces (light rotors, dark stators, location of hub leakages, and shroud bleed also shown)

preserved across interface and periodic boundaries). The main limitation of the TT method is that it formally applies only to one pitch ratio.

Both PT and TT approaches are fully nonlinear and require no a priori specification of frequencies and naturally support flow oscillations, including nonblade passing frequencies (e.g., self-excitation at trailing edge or tip gap flows).

Multistage Modeling. As noted earlier, in order to predict compressor performance, including stability, the entire compressor must be modeled in one simulation (multistage). For steady state simulations this is easily accomplished by using mixing plane interfaces between each rotor-stator pairing.

There are a variety of transient multistage simulation techniques available in the literature, each with different strengths and weaknesses. The nonlinear harmonic method, He [14], solves the time-averaged equations but includes estimates for the deterministic stresses (Adameczyk [15]) based on linearized solutions of Fourier-based perturbations from the mean flow. The harmonic balance method, Hall et al. [16], solves the fully nonlinear true transient equations but in frequency space, based on a predefined set of base frequencies and harmonics.

The current work seeks to obtain a fully nonlinear true transient simulation in the time domain with support for blade passing and self-excitation frequencies (perhaps important in predicting the onset of stall). Several different transient multistage approaches are possible with the CFX [8] solver based on different combinations of TRS interface methods.

Multistage PT. This method uses PT interfaces between all components. In this case the transient flow within each component is time accurate, but flow profiles are distorted (frequency shifted) in proportion to the pitch ratio between components. This approach provides a very good approximation to the true transient flow, avoiding modeling errors incurred by mixing planes. The multistage PT interface model has been a workhorse for “transient multistage” for the past decade.

Multistage TT-MP. This method uses the TT method for each rotor + stator stage and connects stages to one another (the stator-to-rotor interface) using mixing planes. Time accurate transient flow is resolved within each stage and adjacent stages exchange mixed-out flow conditions. This approach accurately resolves local flow instabilities within a stage, but some fidelity is lost between stages. The approach is scalable. For example, if it is known a priori that a particular stage initiates stall, just this stage can be modeled using TT and all others modeled as steady with mixing planes. This approach is demonstrated in a preliminary analysis of the inlet guide vane (IGV) + first stage below.

Table 1 Mesh size and parameters for rotor 1, including an extended outlet region for the analysis

Rotor 1	Coarse	Medium	Fine
Nodes	350,781	1,406,137	5,556,018
Max. aspect ratio	1790	2720	2960
Min. grid angle (deg)	19.35	19.21	19.2
Target Y^+	5	2	1

Multistage TT-PT. This method combines the TT and PT approaches. In this case time accurate flow is resolved within each stage using the TT method, while PT interfaces connect each stage together, as shown in Fig. 2. This method gives a time accurate transient flow simulation through the entire compressor (full time accuracy within each rotor-to-stator stage and approximate time accuracy between stages). While there is some loss in fidelity at the PT interfaces, the temporal variation is well represented. The multistage TT-PT method is demonstrated for the six stage compressor below.

Computational Setup

Geometry and Meshing. Hexahedral meshes were used to economically resolve the boundary layer regions and the tip gap, as well as to permit a sequence of self-similar meshes for mesh dependence studies. Self-similarity of meshes is critical to ensure that any observed difference in successive predictions as the mesh is refined can be attributed to the mesh refinement itself and not to other factors (e.g., unintended changes in the local mesh distribution).

Meshes were carefully constructed to resolve all important areas of the flow: the surface boundary layer, including fillet region and tip vortex, and both blades and vanes must be resolved. Additional axisymmetric domains are defined for leakage and bleed flows, connected to the main gas path by nonconformal interfaces.

Table 1 shows the typical mesh statistics for the first rotor. The medium density mesh targeted approximately 1×10^6 nodes per blade passage. A y^+ of ~ 1 to 2 is achieved on the blade surfaces and end walls, with a smooth coarsening rate away from walls that adequately resolves the boundary layer region with 10 to 20 grid nodes. It is critical that the boundary layer be well resolved to have a chance of predicting the onset of stall, driven by separated flow on the suction surfaces and/or in the tip region. Rotor shroud tip gaps and stator hub tip gaps are highly resolved with 13, 21,

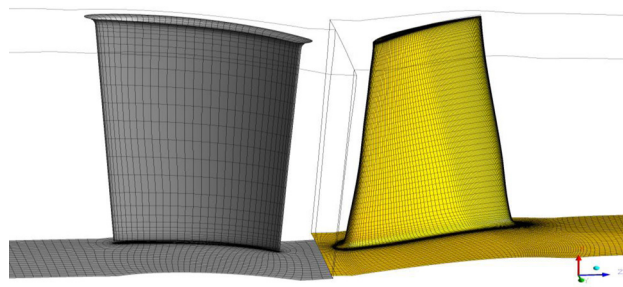


Fig. 3 Computational domain for IGV+R1 analysis on the medium mesh density

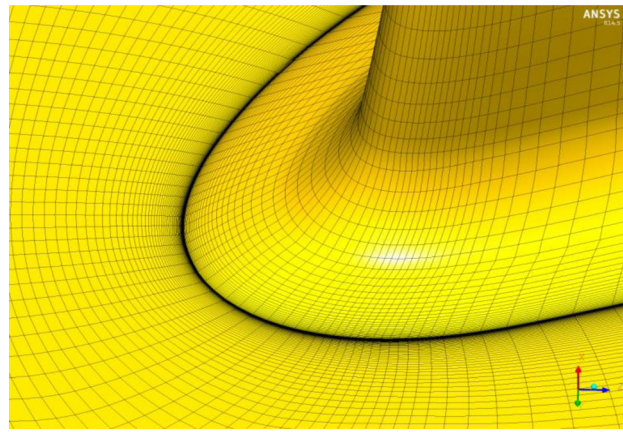


Fig. 4 Zoom-in of leading edge and fillet area of rotor 1 (TurboGrid, fine mesh, distorted view)

and 31 nodes across the gap span for the coarse, medium, and fine meshes, respectively. The blade fillet shape is also accurately resolved by the mesh. Additionally, the grids are a careful balance of resolution between the boundary layers and the midpassage in order to reasonably resolve wakes for the case of unsteady flow simulations.

Figures 3 and 4 show a typical mesh, in this case for the IGV and rotor 1 domains, with a zoom-in showing the meshing in the fillet/leading edge region of a typical rotor (fine mesh density). A total of approximately 13×10^6 nodes were used for the full compressor simulation based on the medium density meshes, which is quite “coarse” given the goal to accurately predict the stability. This mesh size was driven not the least by designer requirements for quick turnaround. A typical performance assessment including the design speed and two different speeds requires ~ 30 simulations per major design variation. Finally, two different mesh generators were used (Numeca AutoGrid and ANSYS TurboGrid) within the project in order to verify that the compressor predictions are independent of mesh style.

Properties and Boundary Conditions. Standard air properties were used, including a variable specific heat (fourth order polynomial of temperature) with thermodynamic consistency for all derived quantities (e.g., Ttotal, Ptotal, static enthalpy, entropy, etc.), Sutherland’s law for conductivity and viscosity, and an ideal gas law for density.

The boundary conditions for the CFD simulations were taken directly from the rig measurements at the corresponding operating condition. At the inlet, circumferentially averaged radial profiles of total pressure and temperature were specified. Likewise the bleed and leakage flows were specified from rig measurements (the mass flow and incoming total temperature were specified as boundary conditions at these locations).

The outflow boundary used either a mass flow or static pressure condition, depending on the situation. For steady simulations either the mass flow or static pressure could be specified, with essentially interchangeable converged results (this compressor is not operated at choked conditions). The mass flow outlet condition implicitly computes the local mass flow distribution based on the approaching flow mass distribution, and the corresponding outlet static pressure level is an implicit result of the simulation (the static pressure meridional shape can be constrained but not its level).

It is highly convenient to specify the mass flow at the outlet boundary for reasons of robustness to stall as well as stable operation when the performance curve is flat or even multivalued away from choke (both the inlet total conditions and the system mass flow can be simultaneously constrained). The mass flow condition is much more stable than a static pressure condition near the stability limit, and generally more robust to startup from simple (1D meanline) initial conditions at any operating point on the speedline. Simultaneous computation of multiple operating points is, therefore, possible, without the need to progress simulations through a sequence of progressively higher operating points. This seemingly minor point is of tremendous practical benefit to the designer for such simulations. All that said, in general it is not possible to specify the mass flow at the outlet when a compressor is choked. In this situation it is necessary to run with the static pressure specified at the outlet. Fortunately, choked flow compressor simulations naturally run reliably and robustly as the system mass flow is again “fixed” but now at a mass flow rate that is an implicit result of the flow prediction.

Transient simulations take their initial conditions from steady (mixing plane) predictions at the same operating point. This practice is essential to minimize the time for transient evolution to quasi-steady flow. Care is also required with the outlet boundary condition choice for transient simulations. The static pressure (average or radial equilibrium distribution) was specified at the outlet and *not* the mass flow. There is a natural oscillation of the mass flow through the machine as the relative position of the rotors and stators change in time. While this oscillation is small for the full 360 deg machine, the oscillation through a given single set of rotor and stator passages per blade row (as defined by the CFD computational domain) is significant. It is nonphysical and inconsistent to fix the system mass flow for all time, implicitly forcing nonphysical pressure oscillations to “maintain” the fixed mass flow as the rotors change relative position. For this reason a temporally constant static pressure outlet boundary condition is specified for all transient simulations. In reality this condition is also incorrect, as the per-passage (local to a specific outlet guide vane (OGV)) static pressure level will oscillate at the outlet, even if the 360 deg machine achieves a very smooth static pressure level with time. The error incurred by assuming local static pressure at one OGV is constant in time is not known.

Preliminary Studies

A preliminary investigation was carried out on the first stage of the six stage compressor. The goal of this portion of the work is to examine the sensitivity of the analysis to numerical, model and systematic errors following the procedures recommended by ERCOFATC Best Practice Guidelines [17]. While operating conditions are taken from the experimental data for the six stage compressor, the primary goal is to examine sensitivity on this simple configuration, rather than compare to experimental data taken from the full compressor. The preliminary study begins by analyzing the IGV+rotor 1, followed by a detailed analysis of the IGV +first stage (rotor 1+stator 1). In both studies the IGV is included in the analysis by a mixing plane interface to rotor 1 to ensure a realistic inlet profile to the rotor. Numerical error is examined (three mesh refinements), various turbulence models are assessed, and tip gap sensitivity is explored, as well as the impact of steady

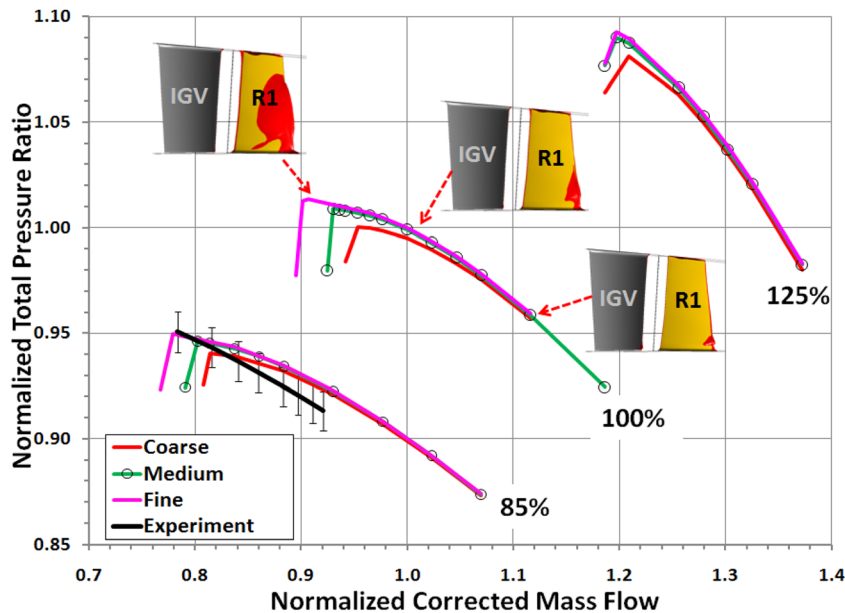


Fig. 5 IGV+rotor 1 performance map (85%, 100%, 120% speedlines) for three mesh densities. Rotor suction side separated flow (black) is shown for three points on the 100% speedline. Experimental data for the six stage compressor is plotted for the 85% speedline (stall set by the 1st stage on this speedline).

and transient simulation approaches. What is learned here is applied to the full compressor analysis.

IGV+Rotor 1 Study. The first study focuses on rotor 1. The computational domain and mesh are shown in Figs. 3 and 4. The experimental inlet profiles are specified upstream of the IGV, and a flow path extension is added downstream of rotor 1 to minimize the impact of the outlet boundary condition. Sensitivity studies focus on the 100% speedline, but the overall performance map was computed (85%, 100%, 120% speedlines) to give context to the observed differences, as shown in Fig. 5. The 85% speedline has the most realistic behavior compared to the experimental rig, as at this low speed the six stage compressor is limited in the first stage, as indicated by Kulite measurements. The experimental characteristic of the first stage is plotted in Fig. 5 for the 85% speedline, only to give some justification to the assumption that the observed CFD error sensitivities for the first stage correlate to a full six stage CFD simulation. The baseline configuration is defined as the medium mesh, the shear stress transport (SST) model with the reattachment model (SST+RM) of Menter [18], and nominal tip gap clearance. The following factors were examined systematically relative to the baseline configuration:

- numerical error: single versus double precision, sensitivity to level of convergence, sensitivity to mesh refinement, sensitivity to first versus second order numerics
- model error: the SST+RM turbulence model was compared to SST, SST Γ - Θ transition (Menter et al. [19]), and the k - ε model (scalable wall functions [8]).
- systematic error: impact of steady versus transient assumption, and tip gap uncertainty

Numerical Error. Three meshes for rotor 1 (Table 1) were defined with refinement of approximately a factor of four between each mesh. Care was taken to ensure self-similar meshes with constant proportion, quality, and distribution, as discussed previously. Second order discretization was used for all equations, including the turbulence transport equations. Preliminary investigations on the finest mesh showed no measurable dependence on single or double precision math; hence, all remaining simulations used single precision.

Solutions are compared to each other on the coarse, medium and fine meshes in Fig. 5 for the 85%, 100%, and 120% speedlines (SST+RM turbulence). Close to the design point (bottom right of the three speedlines) all meshes give essentially identical predictions, an important result in itself. But as the operating point moves towards stall, significant mesh dependence is seen. The predicted peak pressure ratio varies by 0.5% comparing the medium to fine mesh for the 100% speedline, as does its location (fine mesh stalling at 2.5% lower mass flow than the medium mesh). Similar mesh dependence towards stall is seen for the 85% and 120% speedlines.

Mesh dependence cannot be examined independent of the turbulence model. Figure 6 shows the differences in mesh dependence between the SST and k - ε models for the 100% speedline. While mesh dependence is seen for SST (prediction responds as mesh is refined) the k - ε model is essentially mesh independent (all curves are very nearly identical) for all three meshes, in effect “wasting” the well refined boundary layer in the finer meshes. If the boundary layer is resolved into the viscous sublayer, use of the SST is critical to actually give some value from the increased mesh resolution.

Sensitivity to the level of convergence also varies significantly with operating point, as shown in Figs. 7 and 8. Away from stall (e.g., line A), the residuals and the predicted pressure ratio converge tightly in 200 or fewer iterations from a simple 1D initial guess. Towards stall, more iterations are required and tight convergence becomes difficult as separated flow regions periodically form and decay (line B, mass residuals oscillate in a repeating pattern, above machine round off). At the predicted peak pressure ratio, convergence takes about 500 iterations to reach a steady state value, as seen in Fig. 8. Beyond this point (line C, only possible with mass flow specified at the outlet) the simulation takes at least 1000 iterations to converge for both the mass residuals and the pressure ratio. In general great care is required to judge convergence of steady state simulations as stall is approached. Each CFD code, even each turbulence modeling nuance, can impact convergence significantly and its interpretation. There is no substitute for numerical experiment and allowing for long run times even after key performance indicators appear to be stable and constant.

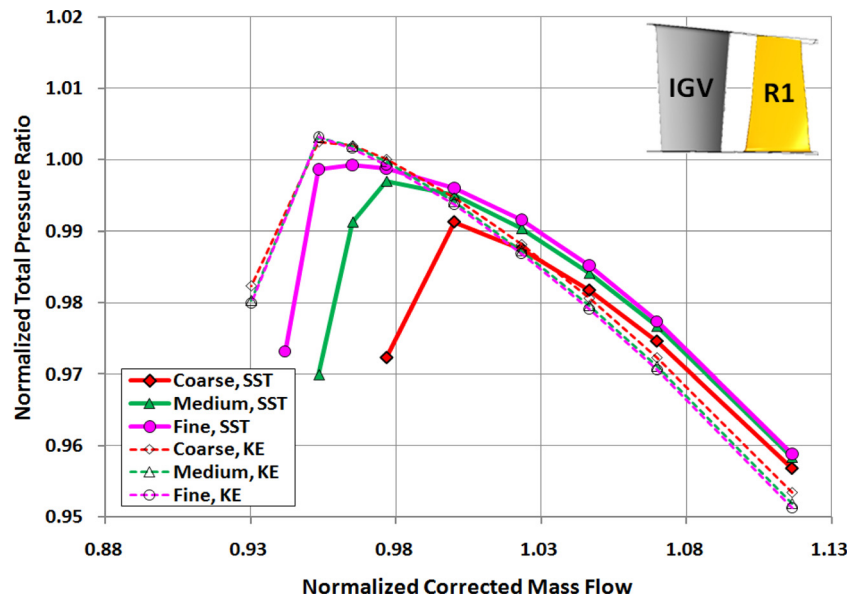


Fig. 6 Comparison of SST (solid) to $k-\epsilon$ (dashed) turbulence versus mesh refinement (100% speedline, IGV+R1)

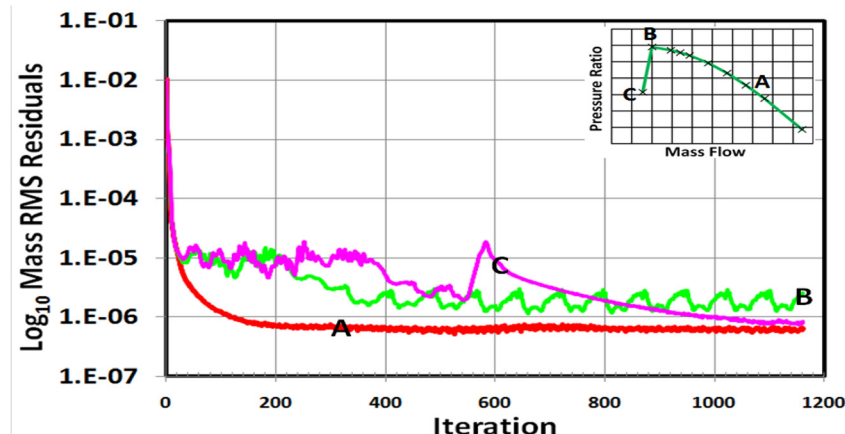


Fig. 7 Differences in convergence rates near design point (A), near stall (B), and stalled (C) for IGV+R1 simulations. The rms mass equation residuals are plotted versus iteration.

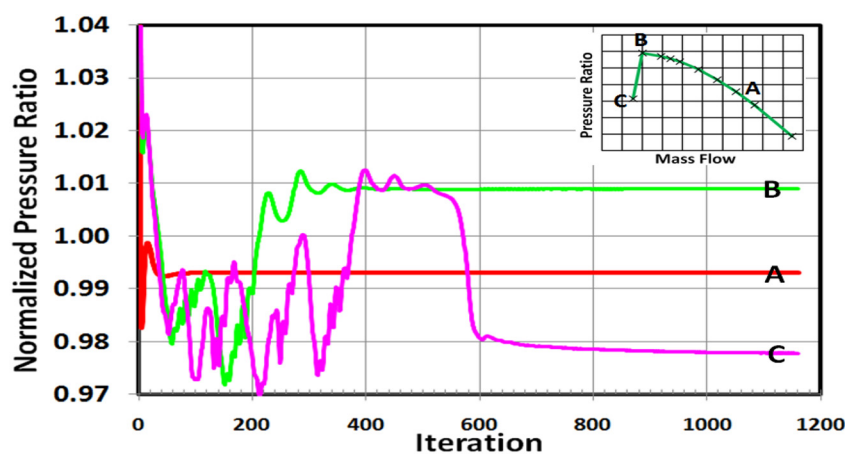


Fig. 8 Differences in convergence rates near design point (A), near stall (B), and stalled (C) for IGV+R1 simulations. The evolving pressure ratio is plotted versus iteration.

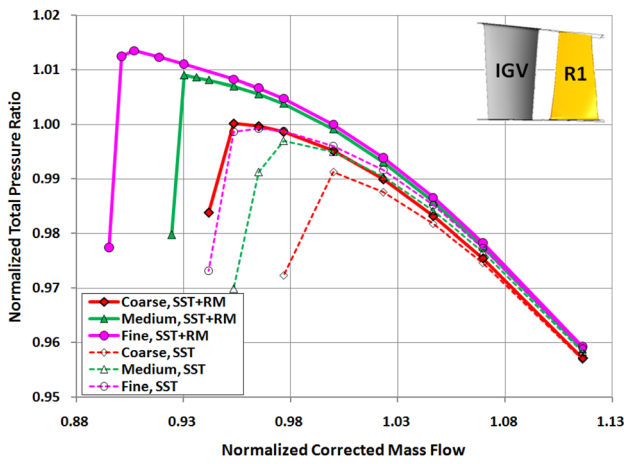


Fig. 9 Comparison of SST to SST+RM turbulence model as a function of mesh refinement (100% speedline, IGV+R1)

Model Error. Turbulence modeling has a major impact on the peak pressure ratio and stall prediction. In this study only Reynolds-averaged Navier-Stokes (RANS)/URANS modeling approaches are considered. Figures 6 and 9 show the sensitivity of SST to $k-\epsilon$, and SST to SST+RM, respectively. As expected, the $k-\epsilon$ model stalls later than the SST model, a well-known fact that $k-\epsilon$ is generally overly optimistic with the onset of separation (falsely delayed). While the SST model is known to more accurately predict the *onset* of separation than the $k-\epsilon$ model, SST can overestimate the growth of a separation bubble once initiated and, therefore, be overly pessimistic at operation with significant stall. The SST+RM model is designed specifically to remedy this situation, more realistically modeling the growth and decay of a separated flow region. Experience on this, and other, compressor cases shows that the stall point prediction from the SST+RM model can give an improvement over the SST model alone and is recommended. This is a key finding observed both in the preliminary IGV+R1 analysis, and confirmed in the full compressor simulations versus experimental data, shown later in this study. Similar observations were made across all three speedlines.

Experiments were also run with the transition model included (SST+RM+transition). Inclusion of transition effects gave a slightly higher peak pressure ratio at a slightly higher mass flow rate but showed much smaller sensitivity compared to the difference between SST versus SST+RM model. In addition, preliminary six stage simulations run with and without the transition model showed essentially no difference in the speedlines and stall point for this compressor. For this reason, the transition model was not used further in this analysis. This is not a general conclusion, however. Inclusion of transition turbulence modeling effects should always be considered and carefully assessed for any compressor analysis.

Systematic Error. Two systematic errors were assessed using the rotor 1 setup: tip gap uncertainty and the imposition of steady state flow. The flow over the blade tip dominates the secondary flow pattern in the rotor 1 passage, and hence, the overall performance is very sensitive to the modeled tip gap size. For example, the impact of tip gap uncertainty in a CFD analysis may be larger than the impact of a steady versus transient model or perhaps larger than the impact of various pitch change models. The actual running tip gap is difficult to ascertain but is perhaps one of the most critical items to assess for systematic uncertainty in any rotor simulation, especially for tip-limited configurations.

It is, therefore, important to assess tip gap sensitivity with CFD simulations. Care was taken to maintain the mesh quality in the tip gap by using identical expansion factors and values of y -plus between the different tip gap mesh sizes. Figure 10 shows the impact of varying the tip gap by $\pm 25\%$ (which is in the range

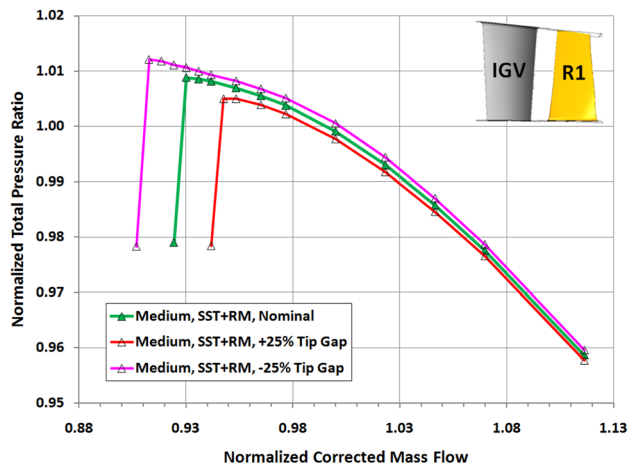


Fig. 10 Sensitivity to tip gap uncertainty comparing nominal gap to $\pm 25\%$ gap (100% speedline, medium mesh, IGV+R1)

of the uncertainty of the tip clearances) of the estimated (tight) tip gap in the experimental rig. Even this small variation in geometry significantly impacts the achieved peak pressure and its location. As expected, the larger tip gap achieves a lower peak pressure ratio at a higher mass flow, and the reduced tip gap achieves a higher peak pressure ratio at a lower mass flow, compared to the nominal tip gap case. Determining peak pressure ratio for the reduced tip gap case was more difficult than for the nominal tip gap, requiring more than 1000 iterations to stabilize (the last two operating points beyond peak pressure ratio oscillated by $\pm 0.3\%$, average value plotted). Close comparison of the reduced tip gap flow to the nominal tip gap flow at the achieved peak pressure ratio shows an enlarged suction side separated flow as well as slightly more turning and loading towards the tip region. These flow feature differences for the reduced tip gap case perhaps explains the observed differences in convergence behavior. Similar tip gap sensitivity was observed with the fine mesh.

Finally, the systematic error incurred by assuming steady flow was assessed. A second order accurate transient simulation (50 time steps per rotor 1 pitch) was performed near surge. The mixing plane between the IGV and rotor 1 remained unchanged, so the only source of unsteadiness was self-induced oscillations from either the tip flow and/or separated flow areas. An unsteady flow developed in the tip region, as well as within the suction side separation bubble (Fig. 5). The observed frequency of oscillation was ~ 4200 Hz, quite independent of the rotor 1 passing period (~ 6000 Hz) while the predicted performance from the transient simulation was nearly identical to that of the steady simulation. The conclusion was the imposition of steady flow assumption for the isolated rotor is a minor error, and the inherent single row unsteadiness has only a small impact. This conclusion is based on a simulation with no rotor-stator interaction modeled. Including transient rotor-stator interaction has a much more significant impact, as discussed in the next section.

First Stage (IGV + R1 + S1) Study. Similar to the rotor 1 study, the computational domain consists of an IGV connected by a mixing plane to the first stage of the compressor (rotor 1+stator 1). The SST+RM model on the medium density mesh was used for all simulations.

A series of simulations were performed across the 100% speedline to examine sensitivity to steady versus a transient rotor-stator analysis. For the steady simulation, a mixing plane interface is defined between rotor 1 and stator 1. For the transient simulation, a fully time accurate time transformation model is used for rotor 1+stator 1, accurately accounting for the R1/S1 pitch ratio (~ 1.17). Initial conditions for all transient simulations were taken from the corresponding steady state simulation. A baseline time

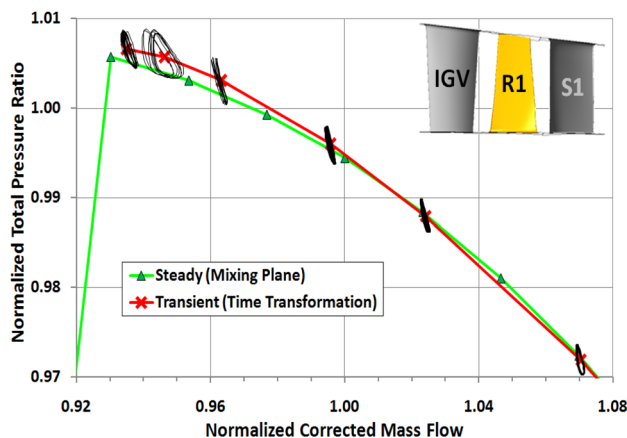


Fig. 11 Comparison of steady (mixing plane) to transient (time transformation) simulations for IGV+R1+S1. The trace of the transient variation over several blade passings is superimposed (thin black lines) to show extent of oscillations.

step of 25 steps per rotor 1 pitch was used for the whole speed line. A time step sensitivity study was also conducted.

The pressure ratio versus mass flow is plotted in Fig. 11 for both steady and transient CFD simulations. At the design point, the steady and transient CFD simulations are virtually identical, but the predictions become progressively different towards stall. The transient simulations reach a higher peak pressure ratio sooner (at a higher mass flow) than the steady simulations, predicting a steeper speedline as surge is approached. Traces of the pressure ratio signal as a function of time are also plotted for the transient simulations at selected operating points, to give an indication of the temporal variation (dashed lines). The transient oscillations grow in size towards stall with the largest oscillation envelope occurring just slightly before the peak pressure ratio. That said, it is encouraging for designers, if not surprising, that the steady and transient simulations are very close throughout most of the operating range.

Sensitivity of the prediction to time step was evaluated at one operating point (near stall). Three time steps were used (corresponding to 25, 50, and 100 time steps per rotor 1 pitch). The results are plotted in Fig. 12, comparing the time trace of the pressure ratio over the last few periods of the simulation. There are differences between the coarse and medium time steps, but very small differences between the medium and fine time steps. Surprisingly, the very coarse 25 steps per period resolve the main transient features of the flow and give very nearly the same overall time-averaged performance.

Finally, it must be noted that a major source of uncertainty in the transient simulations is caused by the use of a URANS turbulence model. The SST model, and variants, is a RANS-based model developed primarily for steady flow simulations. While it is standard practice to use RANS models for globally unsteady flows such as rotor-stator interaction, the URANS approach introduces potentially significant modeling error in unsteady predictions. The extent to which URANS artificially dampens transient flow features important to stall is largely unknown. Future compressor stall studies should assess the importance of scale resolving turbulence models (LES variants). Hybrid models, such as the scale resolving simulation (SAS) model (Menter and Egorov [20]) are attractive in that they retain a RANS approach inside the boundary layer yet resolve large eddies in the passage for a sufficiently resolved mesh and time step.

Preliminary Study Summary. From the rotor 1 and first stage studies, the following summary and recommendations can be made:

- CFD best practices established at design flow conditions do not carry over toward stall. Near stall there are significant

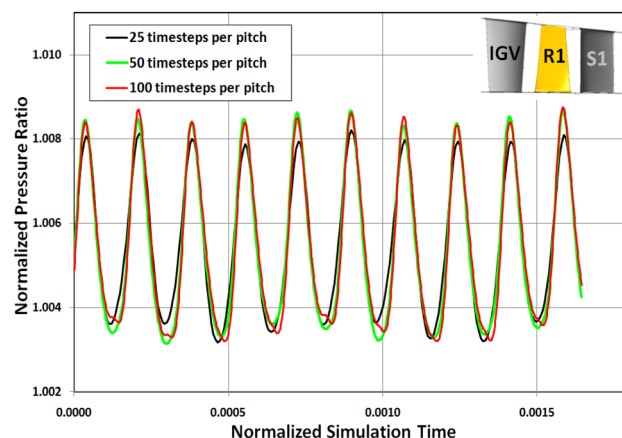


Fig. 12 Sensitivity of simulation to time step size shown, plotting the pressure ratio signal for several cycles, for three time step sizes (25, 50, and 100 time steps per rotor 1 pitch)

regions of separated flow. The solutions are very sensitive to model assumptions. Best practices must be assessed near stall conditions.

- A mesh density of $\sim 1 \times 10^6$ nodes per blade row is excellent at the design point but a minimum recommendation near stall when advanced turbulence models such as SST are used.
- SST with the reattachment model is recommended for compressor simulations near stall. Detailed resolution of the boundary layer flow is critical to accurately predict separated flow regions, pertinent to stall inception. The $k-\epsilon$ model is not recommended.
- Tip gap uncertainty is magnified at the stability limit. Quantify this uncertainty by numerical experiment.
- Transient oscillations at nonblade passing frequencies exist even in an isolated rotor analysis (e.g., from tip flow). Resolution of these frequencies may be important for stall prediction in a multistage machine.
- Differences between steady and transient rotor-stator simulations occur toward stall. Multistage compressor stall simulations will likely be impacted by a transient analysis as well.

These recommendations are generally valid as well as they are applied to the CFD analysis of a multistage compressor, discussed in the next sections.

Six Stage Compressor Analysis

The CFD analysis of the complete six stage compressor is described in this section. Predictions are directly compared to the experimental data as well as between steady and transient approaches. The computational domain consists of an IGV, six stages, an outlet guide vane (OGV), and a diffuser region (CED) as shown in Fig. 2. A second CFD model consisting of the compressor blading only (without the CED) was run for some speedlines to investigate the upstream impact of the CED pressure field on the last airfoils. Mass leakages and bleeds on hub and shroud regions are defined using truncated axisymmetric domains. All boundary conditions are prescribed from the experimental data. Mass flow or pressure is specified at the outlet for steady runs, but static pressure is specified at the outlet for transient simulations. Initial conditions for steady simulations are based on a simple 1D profile of pressure from inlet to outlet. Initial conditions for transient simulations are the steady predictions at the corresponding operating point.

The medium mesh density is used for all blade rows for a total of approximately 13×10^6 nodes. While the medium mesh on the single stage analysis shows mesh dependence near stall in the preliminary study, a compromise was necessary for the current six stage simulations. A goal of the current work was to understand

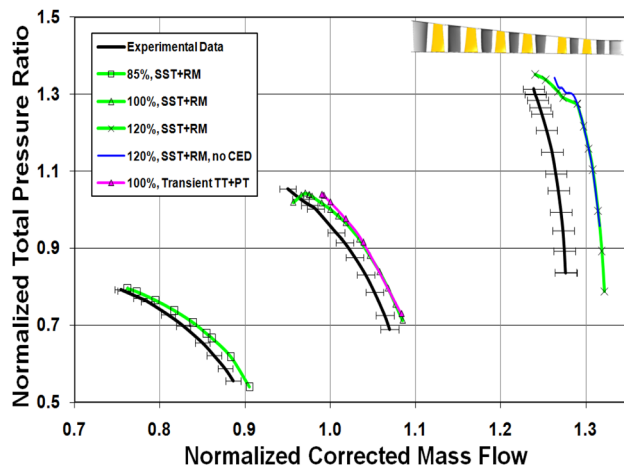


Fig. 13 Six stage compressor, pressure ratio versus mass flow. Steady CFD, transient CFD, and experimental data (black, error bars) are compared for 85%, 100%, and 120% speedlines.

how well one can predict the performance map up to the stall limit, using only 1×10^6 nodes per blade passage. Future study is required to assess the impact of mesh refinement on the six stage simulations. For all simulations, second order spatial and temporal numerics were used for all transport equations, with the exception of first order spatial numerics for the SST model turbulence transport equations.

Steady Simulations. Steady simulations used mixing plane interfaces between each rotor and stator. Three speedlines were computed at 85%, 100%, and 120% of the design speed. On each speedline 10 or more operating points are computed, with larger steps between operating points near the design point and smaller steps as the stability limit was approached.

Steady state performance map predictions across the speedline are shown in Fig. 13 (pressure ratio), Fig. 14 (zoom-in of pressure ratio at 100% speedline), and Fig. 15 (efficiency), including comparison to experimental values. Several observations can be made from these plots:

- Predictions of pressure ratio and efficiency generally compare well to the experimental data, across the full performance map, including the shape of the speedlines from design point to stall.
- A nearly constant shift between predicted and measured mass flow was seen for all three speedlines. The cause of this systematic difference is not yet understood but may be caused by factors such as: systematic error in computing the experimental mass flow, numerical error (insufficient mesh refinement), model error (turbulence) or geometry error in the CFD model. More investigation is required. A similar shift was predicted by two other independent CFD solvers, supporting a systematic cause rather than a code-specific error.
- The peak pressure ratio predicted by the steady simulations is generally very close to the experimental data. On the 100% speedline the steady prediction is within 1% of the experimental peak pressure ratio, which is highly encouraging given the complexity of the flow (stall in last two stages detected by Kulite pressure probes) versus the mesh resolution. Based on the single stage sensitivity studies it could be expected that with finer grids the peak pressure ratio will slightly increase.
- The shape of the steady speedline flattens relative to the experimental data, extending the stall point to a lower mass flow. The mixing plane interfaces effectively reduce the pitchwise variation in the flow during the mixing process at each frame change interface, causing a more gentle approach

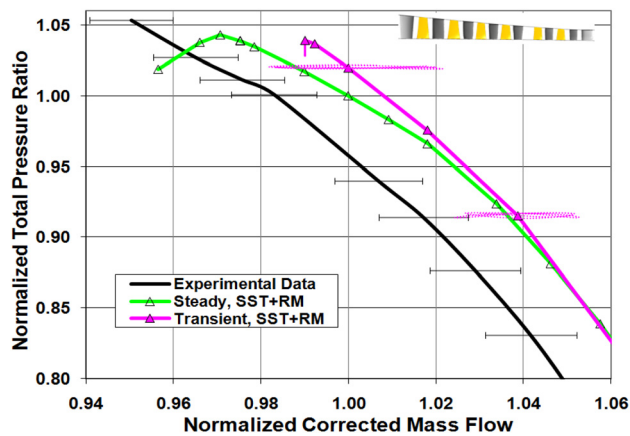


Fig. 14 Zoom-in of 100% speedline, pressure ratio versus mass flow for six stage compressor. Transient CFD signal is plotted (dashed line) for a few blade passings to indicate the extent of the oscillations (growing towards stall).

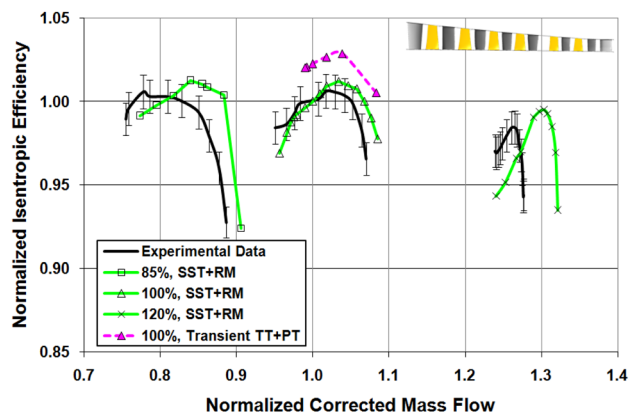


Fig. 15 Six stage compressor map of efficiency versus mass flow. Steady CFD (gray lines), transient CFD (dashed line) and experimental data (black, error bars) are compared for 85%, 100%, and 120% speedlines.

to the peak pressure ratio. The mixing planes artificially redistribute the flow after each rotor, thereby reducing the flow distortion on downstream components.

- The predicted efficiency also compares well to the experimental data. As with the pressure ratio data, there is a shift between the experiment and CFD. The CFD results overestimate the efficiency as not all of the actual losses are represented in the CFD model. The shape of the efficiency characteristics is predicted well, thus changes in loss production at off design are sufficiently captured.
- Each operating point is computed in one to four wall clock hours on a modern cluster running 64 cores, depending on the operating point (1 h for the design point, 4 h near stall). Multiple operating points can be simultaneously and independently computed.
- Modeling the CED has a small impact at the 120% speed line only. At higher speeds the very last rows are limited, thus details of the exit flow are important. Without the diffuser there is a separation approaching the outflow boundary condition, giving a somewhat lower peak PR (blue line on Fig. 13).
- Stall initiates in the first stage for the 85% speedline and in the last stages for the 120% speedline, as illustrated in Fig. 16 (red areas represent regions of separated flow on the suction surfaces). The blade rows in which stall inception is predicted agree well with the experimental observations based on the onset of high amplitude nonblade-passing

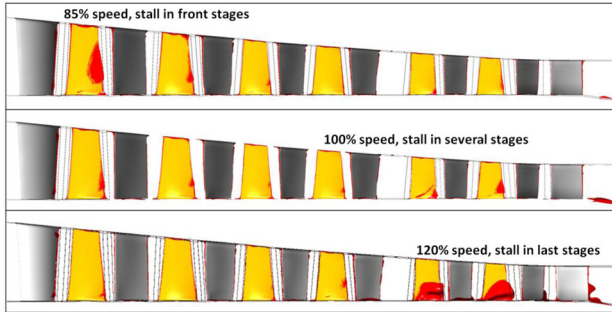


Fig. 16 Visualization of CFD stall regions (suction side of rotors, colored black) at peak pressure ratio. At 85% speed (top) stall initiates mostly in the first stage, at 100% (middle) stall occurs in several stages, and at 120% (bottom) stall is almost exclusively in the last two stages.

frequency Kulite signals and leading edge (LE) instrumentation data close to the peak pressure ratio. Also, changes in the measured radial P_{total} distributions while the compressor is throttled indicate that the last stages are hub limited at high speeds, as predicted by the CFD.

Transient Simulations. TT-PT transient simulations of the entire six stage compressor were made for the 100% speedline from the design point to stall, as shown in Figs. 13–15. Time transformation was used within each stage (rotor-stator pair), and the stages were connected to each other using profile transformation interfaces. A coarse time step of 25 steps per rotor 6 pitch was used. Between 2000 and 2500 time steps were run for most simulations, corresponding to approximately two residence times of the compressor (and more than one full rotation of the compressor). Arguably this is the minimum time integration needed to get meaningful transient results starting from steady initial conditions.

Figure 14 gives a zoom-in of Fig. 13 for the 100% speedline, including a trace of the transient pressure ratio signal for the last few blade passings at two operating points, to give an indication of the extent of the transient oscillations (extent is highly exaggerated as the data are extracted for one passage per blade row but multiplied by the total number of passages in 360). Finally, the complete time evolution of the pressure ratio at the best efficiency point is shown in Fig. 17. More than three revolutions of the compressor were simulated. The following observations about the transient simulations can be made:

- Multiple frequencies are found in the simulation, including the blade passing frequencies as well as others.

- The transient simulations reach a higher peak pressure ratio at a higher mass flow than do the steady simulations but stall at a similar peak pressure ratio.

- The shape and slope of the 100% transient speedline matches the experimental data very closely up to stall (steeper approach to stall than for the steady simulations). In addition, the transient simulations stall abruptly like in the experiment (due to the pressure outlet boundary), whereas the steady simulations actually can extend past peak pressure ratio (due to the mass outlet boundary).

- Multistage transient CFD simulations correctly resolve the buildup of flow disturbances such as wakes, local flow separation, etc., as they propagate downstream from stage to stage, directly impacting the stability prediction when these disturbances increase. Likewise, the importance of transient multistage simulations increases for higher speedlines in order to realistically track and mix-out the location of disturbances between blade rows.

- The transient simulation efficiency is higher than for the steady simulation because the abrupt mixing plane losses are avoided. Transient simulations resolve the gradual mixing-out of blade-to-blade gradients through perhaps multiple downstream stages.

- The transient simulations were at least ~ 50 times more expensive than steady simulations, owing to the increased number of time steps required plus the need to perform subiterations each time step.

Computed and measured radial profiles of P_{total} and T_{total} midway through each stage (upstream of the leading edge of each stator) are shown in Fig. 18 (best efficiency point) and Fig. 19 (near stall) for the 100% speedline. Steady and time averaged transient CFD profiles are compared to the experimental profiles, and in general very good agreement is found. The steady and time averaged transient results are similar to each other at the best efficiency point (BEP), but the transient CFD profiles are noticeably closer to the data for stage 3 and stage 4, where the mass bleed with significantly larger axial gap is located. Obviously the elimination of secondary flow and wakes by the mixing plane has a larger impact for larger axial gaps.

Similarly, Fig. 18 shows that the transient CFD profiles are significantly closer to the experimental data than the steady CFD at near stall conditions, with the notable exception of stage 5. The cause for this difference is not known but may be related to small differences in operating point between experiment and CFD (as stall is approached) and/or unresolved geometric details near the main compressor bleed causing significant local flow differences. More investigation is required. In general the unsteady results show a slightly higher radial mixing that could be expected because the mixing plane virtually eliminates all secondary flow

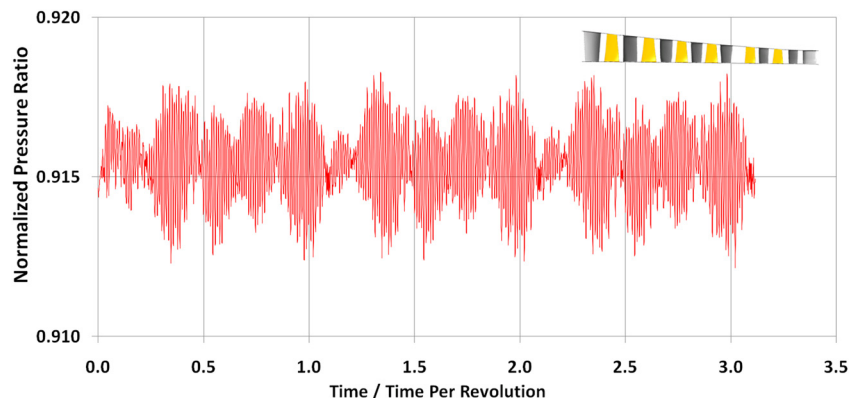


Fig. 17 Time history of the CFD pressure ratio signal as it evolved from steady CFD initial conditions through more than three full revolutions, for six stage compressor (100% speedline, best efficiency point)

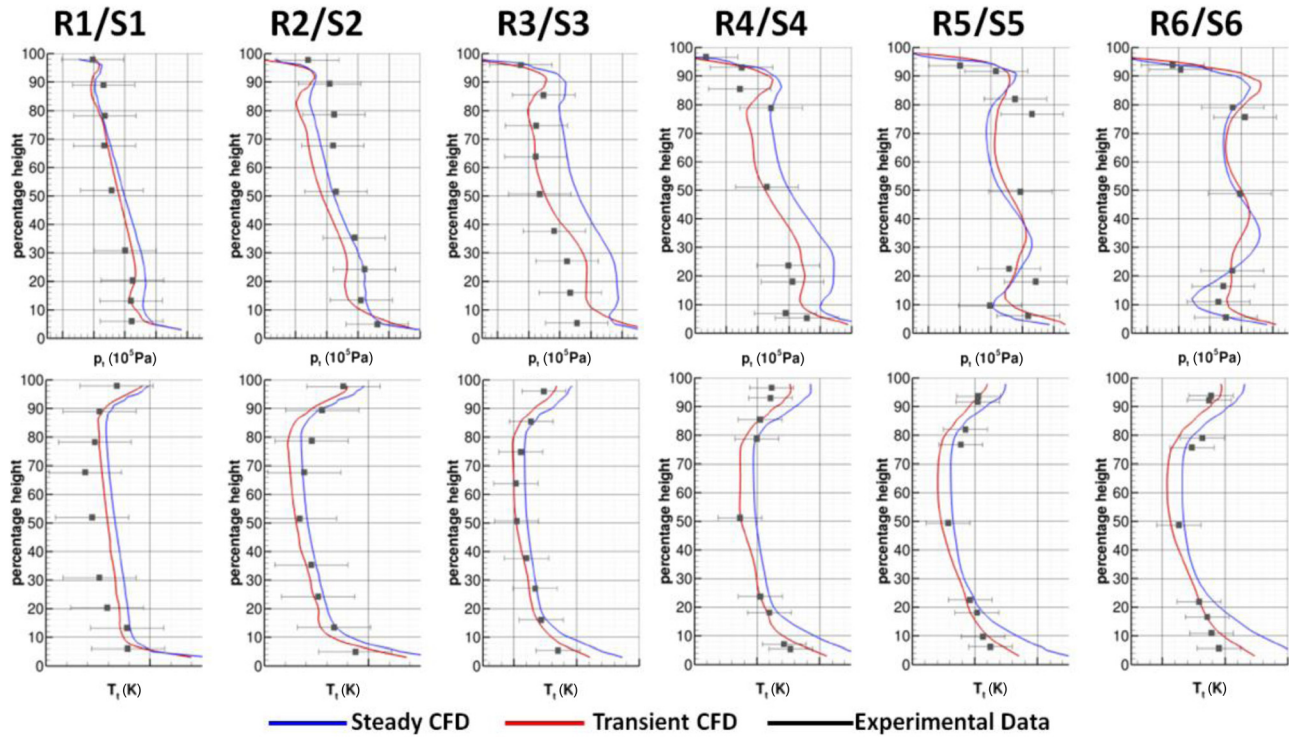


Fig. 18 Radial profiles of P_{total} (top) and T_{total} (bottom) for 100% speedline at *best efficiency point*, measured midway between rotor and stator. Steady and transient CFD results are compared to experimental radial profiles (black, error bars).

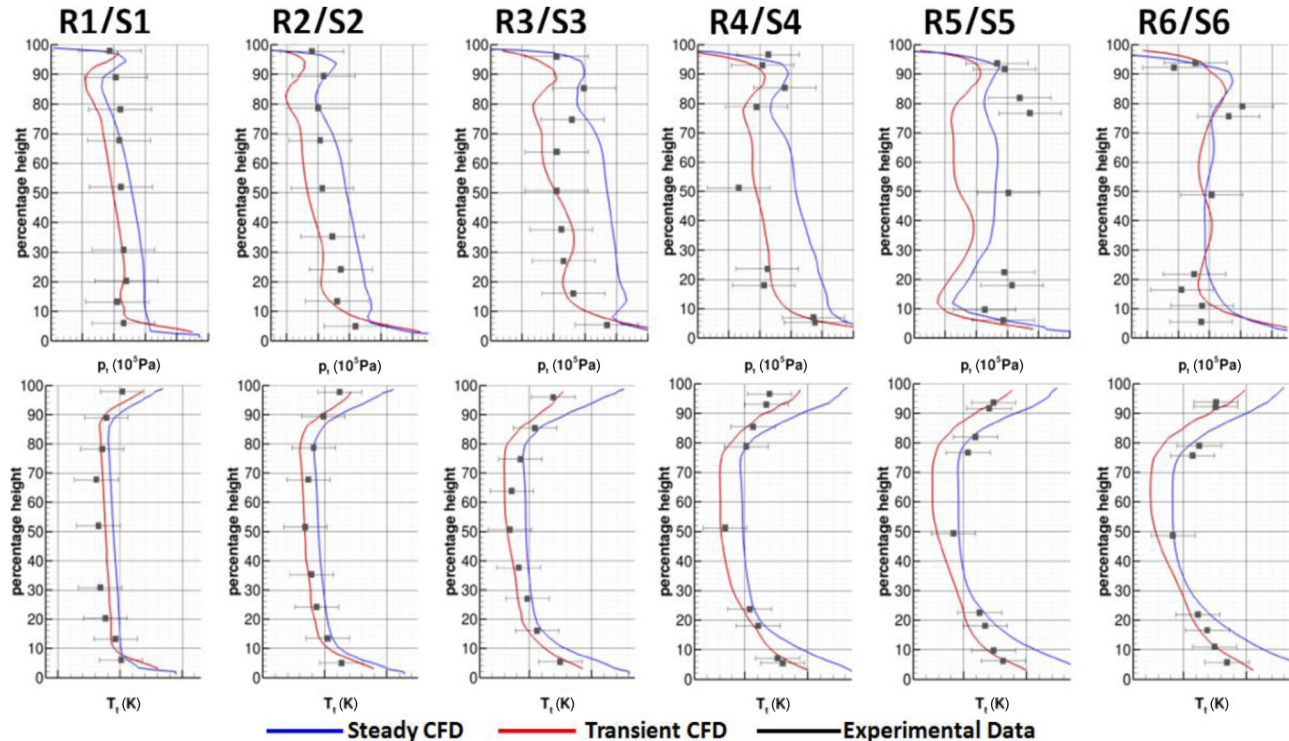


Fig. 19 Radial profiles of P_{total} (top) and T_{total} (bottom) for 100% speedline at *peak pressure ratio*, measured midway between rotor and stator. Steady and transient CFD results are compared to experimental radial profiles (black, error bars).

at the down stream side of the interface. The realistic radial mixing in the transient simulations could be the reason for the stiffer speedlines because the local suction side separations are reduced due to mixing with higher momentum flow from the midspan region.

Summary and Conclusions

The goal of this work was to systematically investigate the application of CFD methods to predict the performance of a compressor. The findings focus on determining best practices for

predictive capabilities of compressor stall and aerodynamic stability. An experimental half scale six stage axial compressor based on the last stages of the Siemens platform compressor (PCO) was used for the study.

Preliminary investigations focused on the first stage of the compressor. Sensitivity of CFD simulations to numerical, model, and systematic errors were examined across the performance map, from design point to stall. Predictions at the design point are relatively insensitive to mesh size, turbulence model, and steady versus transient approaches. Near stall, however, it was found that a mesh size of 1×10^6 nodes per blade passage is marginal, that the details of the turbulence model approach has a major impact, and that geometric details become much more critical. Likewise, the difference between steady and transient predictions is negligible at the design point but grows as stall is approached.

Based on the preliminary analysis, the performance map for the full six stage compressor was predicted using both steady and transient CFD methods. Steady solutions were obtained across all three speedlines (mixing planes between each blade row). Transient simulations were obtained at the 100% speedline (time transformation within each stage, profile transformation between each stage). The transient simulations were very close to the steady state predictions near the design point, but differences grow towards stall. The transient simulations reached higher pressure ratios at lower mass flows compared to the steady simulations and stall at a slightly lower peak pressure ratio.

A systematic shift between experiment and computation was observed, for both steady and transient CFD predictions, but this shift does not adversely impair the usefulness of the results to the design process. The stiffness of the speedline, the shape of the curve, the predicted peak pressure ratios, and peak efficiency points were all in very good agreement with the data. The transient simulations gave a notably steeper speedline towards stall (matching the data) compared to the steady simulations, by avoiding the artificial smoothing of the (increasingly stronger) pitchwise flow variation inherent with any mixing plane model, as stall is approached.

Future work will focus on the key factors identified that affect stall prediction accuracy: a finer mesh may be required for the stage(s) that go into stall first, a refined time step is needed (a coarse time step was used), and important aspects of the turbulence modeling must be explored especially for the transient simulations (impact of URANS versus scale-resolving turbulence models such as the SAS model).

Acknowledgment

The support of Siemens AG and ANSYS Inc. is gratefully acknowledged. The contributions of Kofi Mainoo and Kim Zwienen to some of the simulations contained in this paper as part of their bachelor work are appreciated and acknowledged.

Permission For Use

The content of this paper is copyrighted by Siemens Energy, Inc. and is licensed to ASME for publication and distribution only. Any inquiries regarding permission to use the content of this paper, in whole or in part, for any purpose must be addressed to Siemens Energy, Inc. directly.

Nomenclature

BEP = best efficiency point

CED = compressor exit diffuser

efficiency = $(T_{\text{total,outlet}} - T_{\text{total,inlet}})/(T_{\text{total,inlet}})^{\text{isentropic}} - T_{\text{total,inlet}}$

GV = inlet guide vane

HPA = Siemens subsonic airfoil family

LE = leading edge of blading

LES = large eddy simulation

OGV = outlet guide vane

pressure ratio = $(\text{mass averaged } P_{\text{total,outlet}})/(\text{mass averaged } P_{\text{total,inlet}})$

PT = profile transformation

Ptotal = total pressure

RANS = Reynolds averaged Navier-Stokes

RM = reattachment model

SAS = scale adaptive simulation

SST = Shear Stress Transport turbulence model

TRS = transient rotor-stator interaction

TT = time transformation

Ttotal = total temperature

URANS = unsteady Reynold-averaged Navier-Stokes

References

- [1] Belamri, T., Galpin, P., Braune, A., and Cornelius, C., "CFD Analysis of a 15 Stage Axial Compressor Part I: Methods," *ASME* Paper No. GT2005-68261.
- [2] Ikeguchi, T., Matsuoka, A., Sakai, Y., and Sakano, Y., "Design and Development of a 14-Stage Axial Compressor for Industrial Gas Turbine," *ASME* Paper No. GT2012-68524.
- [3] Mailach, R., and Vogeler, K., 2007, "Unsteady Aerodynamic Blade Excitation at the Stability Limit and During Rotating Stall in an Axial Compressor," *ASME J. Turbomach.*, **129**, pp. 503–511.
- [4] Camp, T. R., and Day, I. J., 1998, "Study of Spike and Modal Stall Phenomena in a Low-Speed Axial Compressor," *ASME J. Turbomach.*, **120**, 393–401.
- [5] Courtiade, N., and Ottavy, X., "Experimental Study of Surge Precursors in a High Speed Multistage Compressor," *ASME* Paper No. GT2012-68321.
- [6] Költer, U., Mönig, R., Küsters, B., and Schreiber, H. A., 2000, "Development of Advanced Compressor Airfoils for Heavy Duty Gas Turbines—Part I: Design and Optimization," *ASME J. Turbomach.*, **122**, pp. 397–405.
- [7] Küsters, B., Schreiber, H. A., Költer, U., and Mönig, R., 2000, "Development of Advanced Compressor Airfoils for Heavy-Duty Gas Turbines—Part II: Experimental and Theoretical Analysis," *ASME J. Turbomach.*, **122**, pp. 406–415.
- [8] ANSYS cfx Version 14.5, 2012, Ansys Inc., Canonsburg, PA.
- [9] Raw, M. J., "Robustness of Coupled Algebraic Multigrid for the Navier-Stokes Equations," 34th Aerospace and Sciences Meeting and Exhibit, Reno, NV, January 15–18, *AIAA* Paper No. 96-0297.
- [10] Galpin, P. F., Broberg, R. B., and Hutchinson, B. R., 1995, "Three-Dimensional Navier Stokes Predictions of Steady State Rotor/Stator Interaction With Pitch Change," Third Annual Conference of the CFD Society of Canada, Banff, Canada, June 25–27.
- [11] Giles, M., 1988, "Calculation of Unsteady Wake/Rotor Interaction," *J. Propul. Power*, **4**(4), pp. 356–362.
- [12] Connell, S., Braaten, M., Zori, L., Steed, R., Hutchinson, B., and Cox, G., "A Comparison of Advanced Numerical Techniques to Model Transient Flow in Turbomachinery Blade Rows," *ASME* Paper No. GT2011-45820.
- [13] Biesinger, T., Braune, A., Campregher, R., Cornelius, C., Godin, P., Rube, C., Schmid, G., and Zori, L., 2010, "Unsteady CFD Methods in a Commercial Solver for Turbomachinery," *ASME* Paper No. GT2010-22762.
- [14] He, L., 1990, "An Euler Solution for Unsteady Flows Around Oscillating Blades," *ASME J. Turbomach.*, **12**, pp. 714–722.
- [15] Adamczyk, J. J., 1985, "Model Equation for Simulating Flows in Multistage Turbomachinery," *ASME* Paper No. 85-GT-226.
- [16] Hall, K., Thomas, J., and Clark, W. S., 2002, "Computation of Unsteady Nonlinear Flows in Cascades Using a Harmonic Balance Technique," *AIAA J.*, **40**(5), pp. 879–886.
- [17] ERCOFTAC, 2013, "The ERCOFTAC Best Practice Guidelines for Industrial Computational Fluid Dynamics," European Research Community on Flow, Turbulence and Combustion, Brussels, Belgium.
- [18] Menter, F. R., 1994, "Two-Equation Eddy-Viscosity Turbulence Models for Engineering Applications," *AIAA J.*, **32**(8), pp. 1598–1605.
- [19] Menter, F. R., Langtry, R., and Völker, S., 2006, "Transition Modelling for General Purpose Codes," *J. Flow Turb. Combust.*, **77**(1–4), pp. 277–303.
- [20] Menter, F. R., and Egorov, Y., 2005, "A Scale-Adaptive Simulation Model Using Two-Equation Models," *AIAA* Paper No. 2005-1095.